Room temperature control of spin states in a thin film of a photochromic iron(ii) complex

Materials Horizons

ARTICLE

Room Temperature Control of Spin States in a Thin Film of a Photochromic Iron(II) Complex

Lorenzo Poggini,*[a,b] Magdalena Milek,[c] Giacomo Londi,[a] Ahmad Naim,[b] Giordano Poneti,[a]‖ Lorenzo Squillantini,[b] Agnese Magnani, [d] Federico Totti,[a] Patrick Rosa,[b] Marat M. Khusniyarov,*[c] Matteo Mannini*[a]

Received 00th January 20xx,
Accepted 00th January 20xx

DOI: 10.1039/x0xx00000x

www.rsc.org/

Thin films of a molecular spin crossover iron(II) complex featuring a photochromic diarylethene-based ligand have been grown by sublimation in ultra-high vacuum on an Au(111) single crystal, and investigated by X-ray and UV photoelectron spectroscopies. Temperature-dependent studies demonstrate that the thermally-induced spin crossover behaviour is preserved in thin films. The photochromic ligand deliberately integrated into the complex allows photoswitching of the spin states of this iron(II) complex at room temperature, and this photomagnetic effect is still observed in 5 nm thick sublimated films. Thus, this work opens new horizons and pushes bistable spin crossover systems closer to prospective applications in molecular electronics and molecular spintronics devices functioning at room temperature

1. Introduction

Spin crossover (SCO) materials feature reversible spin state switching of a metal ion through external stimuli as temperature, light irradiation, pressure, electric and magnetic field.[1,2] In iron(II) complexes, the most investigated class of SCO systems to date, switching occurs between a diamagnetic low-spin state (LS, *S*=0) and a paramagnetic high-spin state (HS, *S*=2), with consequent changes in molecular and electronic structures, and corresponding magnetic, optical, and electric properties.[1,2] Recent studies revealed that SCO systems can retain *switchability* even in nanostructured assemblies, including (sub)monolayers and thin films.[3–22]For these reasons SCO species are thought to be highly promising candidates as active components in prospective spintronics and molecule-based data storage devices[23–25] as well as in innovative devices profiting of additional features obtained by combining SCO with other functionalities.[26,27] this research framework, molecular systems whose magnetic and electronic properties can be reversibly switched at *room temperature* (RT) are particularly attractive.[28] One approach to achieve such switching is to change the coordination number of a metal complex by optical or chemical means, which was demonstrated for cobalt(II/III)[29,30] and nickel(II)[31–33]complexes. Another approach is the optical modulation of the ligand field at the metal ion via a photoreaction at the coordinated ligand, the so called Ligand-Driven Light-Induced Spin Change (LD-LISC) effect.[34–40] Although the latter was proposed 24 years ago,[41] only recently[42,43] SCO photo induced convertion has been observed at RT via LD-LISC. The reported system resulted to be reversible and more efficient compared to previous systems.[44,45] Thus, the molecular complex [$Fe^{II}(H_2B(pz)_2)_2$*phen**] (**1**, *pz* = 1*H*-pyrazol-1-yl, *phen** = a diarylethene-functionalized phenanthroline ligand, Figure 1), has been reversibly switched between HS and LS states at RT in solution[32] and in the solid state.[43] The photoswitching at molecular level is driven by the reversible photocyclization of

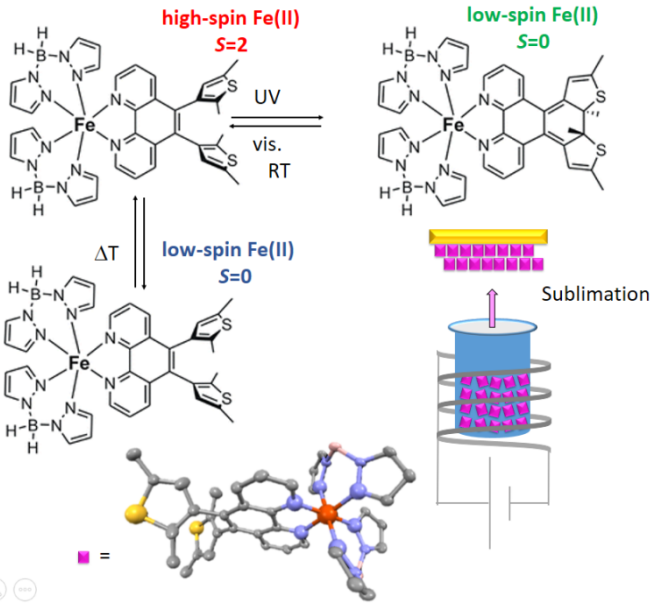

Figure 1. Molecular structure of the [$Fe^{II}(H_2B(pz)_2)_2$*phen**] complex and schematic representation of the UHV sublimation process (bottom). Control of the spin state by room-temperature photocyclization of *phen** ligand and by temperature (top).

Dr. L. Poggini, G. Londi, Prof. G. Poneti, Prof. F. Totti, Dr. M. Mannini
Department of Chemistry "Ugo Schiff" and INSTM Research Unit of Firenze, University of Firenze, I-50019 Sesto Fiorentino, Italy
E-mail: matteo.mannini@unifi.it
Dr. L. Poggini, A. Naim, Dr. P. Rosa CNRS, Univ. Bordeaux, ICMCB, UMR5026, F-33600 Pessac, France
E-mail: lorenzo.poggini@icmcb.cnrs
M. Milek, Dr. M. M. Khusniyarov Department of Chemistry andPharmacy, Friedrich-Alexander University Erlangen-Nürnberg (FAU), Egerlandstr. 1, 91058, Erlangen, Germany. E-mail: marat.khusniyarov@fau.de
Prof. A. Magnani University of Siena, Department of Biotechnologies, Chemistry and Pharmacy, INSTM Research Unit of Siena, Via A. Moro 2, 53100 Siena, Italy
‖Present address: Institute of Chemistry, Federal University of Rio de Janeiro, Av. Athos da Silveira Ramos, nº 149, 21941-909, Rio de Janeiro, Brazil

† Electronic Supplementary Information (ESI) available: Magnetic characterization of the sublimated films; additional XPS and ToF-SIMS characterization; TDOS plot. See DOI: 10.1039/x0xx00000x

the diarylethene-based ligand leading to a HS→LS photoconversion at RT of 40 % in solution and 32 % in the solid state.

The incomplete photoswitching has been attributed to the presence of two conformers of the diarylethene ligand, *i.e.* photoactive antiparallel and photoinactive parallel,[46] present simultaneously in the studied samples. However, because of the perspectives of having a RT convertible SCO system, it is highly tempting to transfer this unique iron(II) molecular photoswitch to surfaces. Indeed, some closely related SCO complexes have been reported to sublimate intact on surfaces [47] and references therein.

We report herein the preparation of ultrathin films (5 nm) of molecular switch **1** obtained via ultra-high vacuum (UHV) sublimation on Au(111) substrates. A well-established protocol already used by some of us for nanosized films of other switchable magnetic molecules[48,49] has been carried out for the characterization of this system at the nanoscale: this multi-technique characterization includes photoelectron spectroscopy, magnetic measurements, and mass spectrometry, in synergy with density functional theory (DFT) calculations. The results obtained have confirmed the preservation of the thermally induced SCO but have also evidenced an unprecedented light-induced SCO in thin films at RT.

2. Results and Discussion

A thin film of ~5 nm corresponding to about 6-8 monolayers of **1** was grown under UHV condition by a thermal evaporation process on Au(111) single crystal prepared by standard sputtering and annealing cycles. The integrity of the molecular switch on the surface was preliminarily verified by time-of-flight secondary ion mass spectrometry, ToF-SIMS, by comparing with a bulk reference (Figure 2). Neglecting matrix effects, similar fragmentation distributions for the bulk sample and for the thin film were observed, including, in particular, three main contributions attributable to the loss of fragments of the two $H_2B(pz)_2$ ligands (a more detailed ToF-SIMS analysis is reported in section S1). An AFM characterization has been carried out in order to confirm a nice defect-free SCO deposit excluding the presence of defective areas or Vollmer-Weber growth. The AFM estimated roughness in an area of 1.6μm^2 resulted about 1.3 nm (Figure S1). Magnetic characterization of the thermally driven SCO in a thicker film (200 nm) on a Teflon substrate has been carried out with a SQUID magnetometer (Figure S2 in ESI). At RT, the $\chi_M T$ product is ~2.4 cm^3·K·mol^{-1}, an intermediate value between the expected ones for a pure HS-Fe^{II} (3.2 – 4.0 cm^3·K·mol^{-1}) and LS-Fe^{II} (≈0 cm^3·K·mol^{-1}), indicating the coexistence of HS (about 70-80 %) and LS species (30-20 %) in the film at this temperature. On cooling, $\chi_M T$ monotonically decreases reaching ~0.8 cm^3·K·mol^{-1} at 50 K and then drops further to 0.3 cm^3·K·mol^{-1} at 2 K due to the zero-field splitting effect on residual HS fraction. Such behavior can be attributed to a very gradual SCO in the film with a residual HS fraction of about 25 – 30 % remaining at low temperatures. A comparison between the thermal switching of the pristine powder sample and the sublimated film (see ESI, section S3) reveals that the nanostructuration has a strong effect on the compound, in particular inducing a much more gradual SCO transition and increasing the residual HS fraction at low temperatures (incomplete SCO). These findings can be tentatively accounted for as resulting from structural inhomogeneities and low degree of elastic interactions among interconverting molecules in the film, similarly to what previously found for doped SCO systems.[50,51]

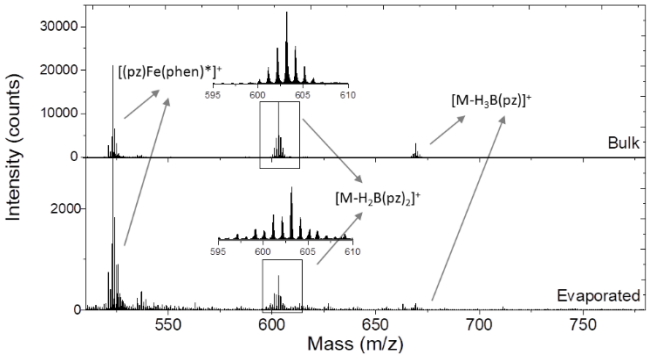

Figure 2. Comparison of the ToF-SIMS mass spectra of **1** (isotopic weight, M= 750.21) in a thin film on Au(111) (top) and in the pristine bulk scratched on Cu (bottom). See Table S1 in ESI for the detailed peak description. *pz* stands for 1*H*-pyrazol-1-yl, *phen** for the diarylethene-functionalized phenanthroline ligand.

Measurements on the thick film irradiated with UV light (λ = 282 nm) evidenced the reversibility of the SCO interconversion but did not reveal significant differences in the thermal transition profile upon photocyclization of the diarylethene ligand (see Figure S3[a] in ESI). We ascribe this to very strong absorption of **1** at 282 nm leading to a severe penetration depth problem for a 200 nm film. Similar problems were identified for solid samples studied previously. [43]

Importantly, SCO in the thick film of **1** can be triggered at low temperature (10 K) also with optical stimulus: irradiation with 532 nm laser light increased the $\chi_M T$ product from 0.73 to 1.03 cm^3·K·mol^{-1} (LIESST effect), leading to the population of a metastable HS Fe^{II} state for about 24 % in the film.[52] This photoswitching can be repeated by the cyclic application of optical and thermal stimuli (see Figure S3[b] in ESI).

To further confirm the successful sublimation of **1** in UHV, we used XPS semiquantitative analysis on a 5 nm thin film (Table S2 in ESI). Considering the limit of the XPS technique (5 % relative error), the experimental data are in excellent agreement with the expected stoichiometry for the pristine complex. Note that sublimation in UHV was successfully used to prepare thin film and monolayer of structurally related but lighter Fe(II) complexes.[5,7–11,13,14,53] XPS has also been used previously to follow, down to the nanoscale, the spin state evolution due to external stimuli. According to earlier literature reports, SCO in bulk[54,55] and thick films[56] can be monitored by using XPS at the Fe*2p* region.

In the present work, thermally-driven SCO has been directly observed in the thin films of **1** by studying the variation of the Fe*2p* peaks line shape at 300 and 150 K (Figure 3a). Differences in the line-shape of Fe *2p* recorded spectra, position of

extracted components and their relative intensity (see table in Figure 3) point to thermally induced SCO in the film. In particular, the reversibility of the SCO transition by the temperature, becomes evident by considering the shape of the Fe$2p_{3/2}$ peak centered at 710.5 eV at RT when the HS state is dominating. Upon cooling, this peak becomes narrower, as expected for the contribution of a LS configuration, in which the coupling of the photoelectron with the partially-filled metal shell during the time of flight following ionization is occurring.[57] Upon warming back to RT, the initial line-shape is re-established and the reversibility of the transition is also confirmed by monitoring the resulting variation in the spin-orbit splitting (ΔE_{SO}): 13.4 eV and 12.4 eV at 300 and 150 K respectively (Figure 3 and table), well in agreement with previous reports for HS and LS components.[10,54,56] Indeed, the ΔE_{SO} changes upon SCO due to different orbital populations in the two spin states: in the HS configuration the measured transition involves e_g-like type d-orbitals that are unoccupied in the LS state.

A deconvolution analysis has been employed to follow the reversible thermally-driven SCO more carefully (Figure 3, bottom and section S4 in ESI). By monitoring the components (highlighted in green, Figure 3a) at 709.4 eV and 721.9 eV (A and A', respectively) univocally attributable to the LS state, [58] we confirm an incomplete but reversible thermal switching. A rough estimation of the conversion efficiency can be obtained by combining this fitting analysis with the $\chi_M T$ curve (Figure S2a): one can safely estimate that a thermal conversion of ca. 25±5% of molecules forming the film is occurring by cooling down from room temperature to the lowest achievable temperature accessible by the used XPS setup (about 150K).

We stress that this thermally driven SCO is an entropy-driven process[42] and does not involve the photo-cyclization of the *phen** ligand. This can be confirmed by monitoring the *S2p* region, which is identical at 300 and 150 K (Figure 3b). Thus the *phen** ligand retains its ground open-ring configuration (*phen*-o*) during the thermal cycles. The S*2p* signal appears centered at 164.9 eV in agreement with literature data.[59,60]

We investigated further the switching of the same 5 nm film this time via UV light irradiation at RT in an *in situ* XPS experiment (Figures 3a and 3b, bottom). The film irradiated with UV light (λ = 282 nm) for 8 h and measured at 300 K reveals an evolution of the Fe*2p* region resembling closely the changes seen during the thermally induced HS-to-LS transition. Indeed, the LS contribution, estimated using the same fitting procedure as described above, is almost doubled (8.9 %) after UV irradiation as compared to the pristine film measured at RT (5.1 %). Thus, the XPS analysis provides evidence for the photoswitching of a sublimated SCO thin film at RT. Importantly, this unprecedented light-induced SCO is triggered

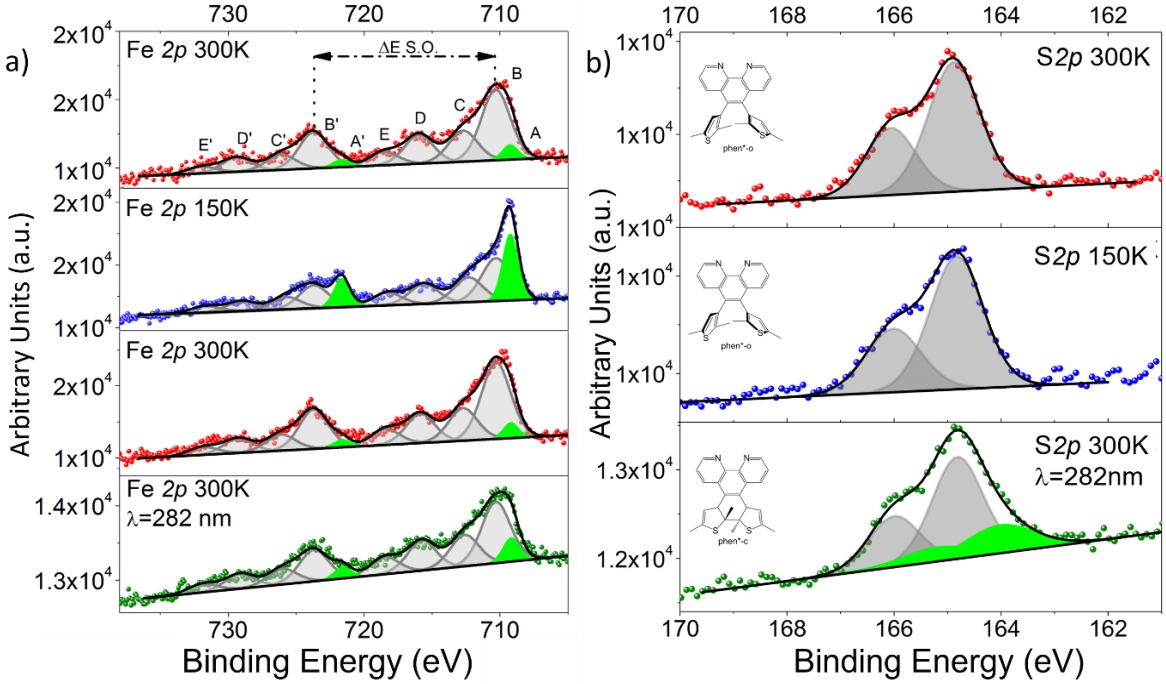

Components	A+A'	B+B'	C+C'	D+D'	E+E'
	%; B.E. (ΔE_{SO})	%; B.E. (ΔE_{SO})	%; B.E. (ΔE_{SO})	%; B.E. (ΔE_{SO})	%; B.E. (ΔE_{SO})
300K	5.10%; 709.26eV (12.4 eV)	46.70%; 710.51 eV (13.4 eV)	20.20%; 712.88 eV (13.4 eV)	19.10%; 715.94 eV (13.4 eV)	8.9%; 718.43 eV (13.4 eV)
150K	24.90%; 709.24 eV (12.4 eV)	32.60%; 710.30 eV (13.4)	18.30%; 712.31 eV (13.4)	14.80%; 715.6 eV (13.4)	9.40% 18.30 eV (13.4)
300K + λ282nm	8.90%; 709.18 eV (12.4 eV)	40.20%; 710.30 eV (13.4 eV)	20.30%; 712.60 eV (13.4 eV)	19.50%; 715.75 eV (13.4 eV)	11.10%; 718.40 eV (13.4 eV)

Figure 3. Top: temperature dependence of the Fe*2p* a) and S*2p* b) peaks for a 5 nm film of **1** evidencing reversible thermally-induced SCO and the effect of UV irradiation at RT. Bottom: spectral components employed for least squares fitting of the Fe*2p* XPS Binding Energies (B.E.). Integrated areas are reported in percentages for each component. Spin-orbit splitting values (ΔE_{SO}) are reported in brackets.

remotely by the photoreaction at the *phen** ligand.[42,43] The UV-induced cyclization of the open-ring isomer *phen*-o* yields a closed-ring isomer (*phen*-c*). The increased LS fraction suggests that the latter produces a stronger ligand field at the coordinated iron(II) ion and triggers a HS-to-LS transition (LD-LISC effect). In this case, being not available the magnetization data, only a rougher estimation based on the percentage of converted molecules by temperature can be obtained evidencing that about 5±1% of molecules are converting at with UV light irradiation at 300 K.

The ligand-based photocyclization is confirmed by monitoring the S*2p* region (Figure 3b). Thus, in addition to the parent component due to *phen*-o* at 164.9 eV (spin-orbit coupled component at 166 eV), the UV-irradiated thin film reveals an additional component (~25±5 %) at lower binding energy (164 eV, spin-orbit coupled component at 165.2 eV). The component at 164 eV is in excellent agreement with the binding energy reported for a closed-ring *phen*-c*.[43] It is worth mentioning that the UV-induced converted Fe(II) molar fraction in the thin film is lower than the ones found for photoswitching in solution[42] and in the solid state[43] for the same complex. While penetration depth issues were thought to be improved with an ultrathin film, the lower efficiency found in the thin film may point towards either a smaller fraction of the photoactive antiparallel conformer of phen* or adverse packing effects in the film at the nanoscale.

A further confirmation of layer by layer growth with good roughness is given by the ultraviolet photoelectron spectroscopy (UPS) analysis carried out as a function of the thickness of the deposited molecules from 0.7 nm to 5.3 nm (ESI, Figure S5): while approaching the final thickness the almost complete attenuation of the gold valence band (VB) is clearly evident, thus excluding the presence of bare gold areas. More importantly, UPS provides additional evidences of the thermal conversion as well as of the partial photoswitching of thin films of **1** at RT. This characterization, performed on the pristine film at 300 and 150 K and after UV-irradiation at 300 K was compared with a DFT-based modelling that contributed to clarify the observed effects. The UPS spectrum acquired on a 5 nm film at 300 K (Figure 4 top) evidences relevant signals at -2.3 eV (band-I), -4.5 eV (band-II), -6.5 eV (band-III), and two very broad features centered at about -9.4 and -14.5 eV, in agreement with similar systems.[10,14,61] The temperature effect on the UPS spectra is visible mainly in the valence-Fermi region (here called A region) for band-I and band-II. Indeed, upon cooling from 300 to 150 K, we observe an increased intensity for band-I, a shift toward higher energies (-2.3 to -2.2 eV) and a less intense band-II (Figure 4 middle). However, the absence of significant changes also in the semi-core (B) and core (C) regions of the spectra suggests that at 150 K the HS component is still present, which is in agreement with the XPS data. Upon UV light irradiation, a significant shift to lower energies (-2.4 eV) is observed for band-I compared to the one recorded for a pristine film at 300 K. Due to the shift to low-energy, band-I in the irradiated sample becomes a shoulder, rather than the well separated band observed for the pristine film. We attribute this change predominantly to the photocyclization of the phen* ligand, which leads to the electronic rearrangement in the valence and Fermi regions. Indeed, similar changes were reported for the photocyclization of organic diarylethenes.[62,63]

The band-II is slightly affected by the cyclization giving an even slighter reduction in energy compared to 150 K. Moreover, minor changes in the relative intensities of bands in the regions B and C were also observed in the UV-irradiated film.

In order to clarify and to quantify the UPS results, DFT calculations on the thermo- and photoswitchable system **1** were performed. The density of states (DOS) for three species have been computed: open-ring HS complex (**1^{HS}-o**), open-ring LS complex (**1^{LS}-o**), and the closed-ring LS complex (**1^{LS}-c**). For the open-ring species **1^{HS}-o** and **1^{LS}-o** both parallel and antiparallel conformers[37] were calculated but no significant differences in the DOS features have been found (Figure S4 in ESI). The computed DOS of the three species shows very similar features in regions B and C, but differ significantly in the region A. Indeed, band-I becomes more intense and redshifted by passing from **1^{HS}-o** to **1^{LS}-c**. Opposite trends are computed for band-II. Therefore, Fermi and valence regions

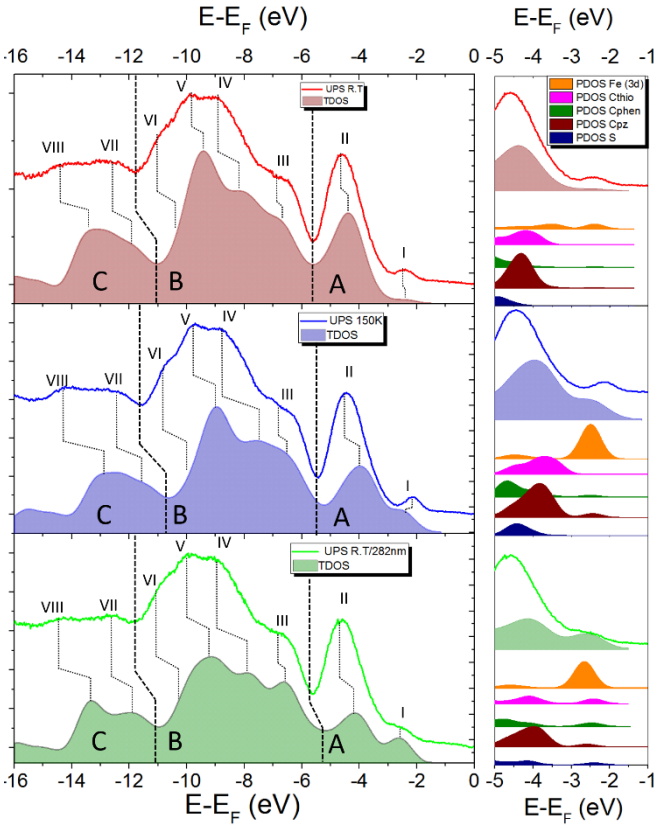

Figure 4. UPS spectra and DOS simulations. Left panel: comparison of the experimental and theoretical data in the region from -14 eV to 0 eV (E-E$_F$) at RT (red, top, TDOS for **1^{HS}-o**), 150 K (blue, middle, TDOS for **1^{LS}-o**) and after UV irradiation (green, bottom, TDOS for **1^{LS}-c**). Right panel: zoom of region A of each spectrum with the calculated projected-DOS.

can be used as fingerprints for different species, allowing a qualitative analysis of the UPS spectra through the computed DOS features in the energy region A. Thus, the DOS calculated for **1^{HS}-o** shows a very good agreement with the spectrum

obtained on a pristine film at 300 K, supporting the major presence of the HS species at RT. The comparison of the UPS spectrum recorded at 150 K with the DOS computed for **1^{HS}-o** and **1^{LS}-o** supports the previous conclusion that a large fraction of HS species is still present at this temperature. In the case of 100 % HS-to-LS conversion, band-II would decrease in intensity and band-I would become redshifted more significantly as observed experimentally.

DFT-based analysis of the UPS data obtained at 300 K after UV irradiation evidences that, although the presence of open-ring HS species is expected to be still relevant, the redshift observed for band-I and the intensity decrease of band-II are in agreement with the presence of **1^{LS}-c**. To shed some light on the origin of band-I and band-II, projected Density of States (pDOS) have been calculated. The resulting contributions are given in the right panel of Figure 4. With regards to band-I, the dominant contribution of *d*-orbitals of the Fe^{II} ion (Fe(*3d*)) is evident in all three considered cases. The rearrangement of *d*-electrons of Fe^{II} due to the HS→LS transition induces an energy redshift on band-I and an increase of its intensity. On the contrary, band-II results from the convolution of several carbon atoms contributions, with the major contributions due to pyrazolyl (C-pz) and thiophenyl (C-thio) carbons. When photocyclization occurs (**1^{LS}-c**), minor contributions of all kind of carbon atoms including the one of the *phen*-c* ligand (C-phen) appear in the Fermi region. Thermally-induced transition can be noticed by the blueshift of the carbon atoms contributions to band-II, while the light-induced SCO, is expected to led to a splitting of the thiophenyl carbon and sulphur (S) contributions. Overall, band-I seems to be more sensitive to the spin state of iron(II) than band-II. Therefore, band-I can be used as a "marker" to monitor both temperature-driven and light-induced SCO in iron(II) species. These effects are qualitatively observed in the reported UPS data thus confirming both the temperature induced SCO and the light-induced conversion at RT.

Conclusions

Spin-crossover molecular switch **1** featuring a photoactive diarylethene-based ligand was successfully evaporated in ultra-high vacuum to form thin films on Au(111). The integrity of the physisorbed complex was confirmed by mass spectrometry, XPS and DFT-supported UPS experiments. Besides thermally induced reversible switching, an unprecedented light-induced spin crossover at room temperature was achieved in thin films. This unique photoswitching is due to the photocyclization of the diarylethene-based ligand, which triggers spin crossover of the coordinated iron(II) ion remotely. Thus, this work opens new horizons for controlling magnetic properties of materials at the nanoscale down to the molecular level at room temperature.

Experimental Section

Experimental Details. **1** has been synthetized following the procedure described elsewhere.[42] The molecular deposit was prepared under UHV conditions by sublimation on an Au(111) substrate, freshly prepared using a standard procedure involving a sputtering and annealing procedure, and then maintaining a pressure of $1x10^{-10}$ mbar during the thermal sublimation of the complex. The sublimation of **1** was carried out at 425 K using a home-built quartz Knudsen cell and the nominal thickness was estimated using a quartz crystal microbalance (QCM). In parallel, as reference, bulk samples characterizations have been obtained by scratching the pristine powder on a Cu foil.

Direct current magnetic investigations were performed using a Quantum Design MPMS instrument equipped with a 5 T magnet. The temperature dependence of the magnetization (M_M) was followed from 1.8 to 300 K by applying a 5 T field from 300 to 45 K and a 0.5 T field below 45 K to reduce magnetic saturation effects. Magnetic susceptibility per mole (χ_M) was then evaluated as $\chi_M = M_M/B$. Magnetic data were corrected for the sample holder contribution and for the sample diamagnetism using Pascal's constants. [64]

ToF-SIMS analysis was carried out with a TRIFT III time-of-flight secondary ion mass spectrometer (Physical Electronics, Chanhassen, MN, USA) equipped with a gold liquid-metal primary ion source. Positive ion spectra were acquired with a pulsed, bunched 22 keV Au^+ primary ion beam, by rastering the ion beam over a 100 µm x 100 µm sample area. The primary ion dose was kept below 1011 ions/cm^2 to maintain static SIMS conditions. All the mass spectra were calibrated to CH_3^+ (m/z 15.023), $C_2H_3^+$ (m/z 27.023), $C_3H_5^+$ (m/z 41.039).

Core-level XPS spectra were acquired with monochromatic Al K_α radiation ($h\nu$ = 1486.7 eV) and a SPECS Phoibos 150 electron analyzer. 40 eV pass energy was used to ensure proper resolution and reliable semi-quantitative analysis. Spectra were taken in normal emission with the X-ray source mounted at an angle of 54.74° with respect to the analyzer. The binding energy scale was calibrated by locating the substrate Au $4f_{7/2}$ peak at 84.0 eV. UPS spectra were measured using the He II line (40.8 eV) from a non-monochromatized gas discharge lamp and the same analyzer used for XPS, yielding an energy resolution of 0.18 eV. A fixed bias of -30 V was applied to the sample to ensure that all the photoelectrons were detected. The spectra were taken in normal emission, and they were energy calibrated using the Au Fermi level.

The variable temperature experiment was performed by using a liquid nitrogen-based cryostat connected to the XPS sample holder. Every spectrum represented herein results from averaging 4 spectra collected after one hour of thermalisation at a specific temperature. The stoichiometry was calculated by peak integration, using theoretically estimated cross-section for each transition.[65] The semiquantitative analysis has been estimated by areas of the deconvoluted peaks. The components were estimated using a fit procedure involving Gaussian-Lorentzian line-shapes, the background in the spectra was subtracted by means of a linear function. UV irradiation of the film was performed *in situ* using a deuterium lamp (20 W) equipped with a bandpass filter (282±5 nm).

Calculation details. All calculations were performed with the CP2K program package[66] within the DFT framework.[67–69] Nonlocal functional was added in order to account for the

long-range dispersion van der Waals interactions. DZVP-MOLOPT (double-ζ polarized molecularly optimized) basis sets were chosen for all the atomic species along with norm-conserving Goedecker-Teter-Hutter (GTH) pseudopotentials. [70] Since no crystallographic data are available for adsorbed **1**, isolated geometry of $\mathbf{1}^{HS}$**-o**, $\mathbf{1}^{LS}$**-o**, and $\mathbf{1}^{LS}$**-c** were used inside a fully periodic simulation cubic cell of 20 Å per side. A large energy cut-off of 550 Ry was applied to the plane-wave basis set. The geometry of $\mathbf{1}^{LS}$**-c** was obtained by imposing the cyclization of the structure forcing the initial geometry.

The geometry optimizations were performed using the GGA revPBE[71] energy functional with the BFGS algorithm and a convergence accuracy on nuclear forces of 4.5×10^{-4} Hartree $Bohr^{-1}$. A convergence threshold criterion on the maximum gradient of the wavefunction in the SCF procedure of 3×10^{-6} Hartree was used applying a Fermi-Dirac distribution with a broadening (electronic temperature) of 3000 K. The density of states (DOS) for the three states of **1** were computed on the revPBE optimized structures by performing single point calculations using a "revised" B3LYP functional,[67,68] which includes an amount of 15 % of the Hartree-Fock exchange, instead of the ordinary 20 %. The choice of reducing the Hartree-Fock exchange amount was made accordingly to previous works.[72] The computed DOS were convoluted with Gaussian functions with a full width half-maximum (FWHM, σ) of 0.6 eV, while all the projected density of states (PDOS) were convoluted with a σ of 0.35 eV for a better distinction of different atomic contributions.

Acknowledgements

We acknowledge the financial contribution of the Ente Cassa di Risparmio di Firenze for the support of the CeTeCS activities. MMK thanks the Deutsche Forschungsgemeinschaft (DFG grant 279-3/1) and the Fonds der Chemischen Industrie (FCI, Liebig Fellowship) for financial support, and Prof. Karsten Meyer (FAU Erlangen-Nürnberg) for his general support. PR and AN acknowledge the financial support of ANR-CHIROTS (n° ANR-11-JS07-013-01), CNRS, Université de Bordeaux and Région Nouvelle Aquitaine.

References

1 P. Gütlich and H. A. Goodwin, *Spin Crossover in Transition Metal Compounds I-III*, Springer-Verlag, Berlin/Heidelberg, 2004, vol. 233–235.

2 M. A. Halcrow, *Spin-Crossover Materials: Properties and Applications*, John Wiley & Sons Ltd, Oxford, UK, 2013.

3 M. Gruber, T. Miyamachi, V. Davesne, M. Bowen, S. Boukari, W. Wulfhekel, M. Alouani and E. Beaurepaire, *J. Chem. Phys.*, 2017, **146**, 92312.

4 W. Kuch and M. Bernien, *J. Phys. Condens. Matter*, 2017, **29**.

5 T. Palamarciuc, J. C. Oberg, F. El Hallak, C. F. Hirjibehedin, M. Serri, S. Heutz, J.-F. Létard and P. Rosa, *J. Mater. Chem.*, 2012, **22**, 9690.

6 T. Miyamachi, M. Gruber, V. Davesne, M. Bowen, S. Boukari, L. Joly, F. Scheurer, G. Rogez, T. K. Yamada, P. Ohresser, E. Beaurepaire and W. Wulfhekel, *Nat. Commun.*, 2012, **3**, 938.

7 T. G. Gopakumar, F. Matino, H. Naggert, A. Bannwarth, F. Tuczek and R. Berndt, *Angew. Chemie - Int. Ed.*, 2012, **51**, 6262–6266.

8 M. Bernien, D. Wiedemann, C. F. Hermanns, A. Krüger, D. Rolf, W. Kroener, P. Müller, A. Grohmann and W. Kuch, *J. Phys. Chem. Lett.*, 2012, **3**, 3431–3434.

9 A. Pronschinske, Y. Chen, G. F. Lewis, D. A. Shultz, A. Calzolari, M. B. Nardelli and D. B. Dougherty, *Nano Lett.*, 2013, **13**, 1429–34.

10 A. Pronschinske, R. C. Bruce, G. Lewis, Y. Chen, A. Calzolari, M. Buongiorno-Nardelli, D. A. Shultz, W. You and D. B. Dougherty, *Chem. Commun.*, 2013, **49**, 10446.

11 T. G. Gopakumar, M. Bernien, H. Naggert, F. Matino, C. F. Hermanns, A. Bannwarth, S. Mühlenberend, A. Krüger, D. Krüger, F. Nickel, W. Walter, R. Berndt, W. Kuch and F. Tuczek, *Chem. - A Eur. J.*, 2013, **19**, 15702–15709.

12 B. Warner, J. C. Oberg, T. G. Gill, F. El Hallak, C. F. Hirjibehedin, M. Serri, S. Heutz, M. A. Arrio, P. Sainctavit, M. Mannini, G. Poneti, R. Sessoli and P. Rosa, *J. Phys. Chem. Lett.*, 2013, **4**, 1546–1552.

13 X. Zhang, T. Palamarciuc, J.-F. Létard, P. Rosa, E. V. Lozada, F. Torres, L. G. Rosa, B. Doudin and P. A. Dowben, *Chem. Commun.*, 2014, **50**, 2255.

14 E. Ludwig, H. Naggert, M. Kalläne, S. Rohlf, E. Krçger, A. Bannwarth, A. Quer, K. Rossnagel, E. Kröger, L. Kipp and F. Tuczek, *Angew. Chem. Int. Ed. Engl.*, 2014, **53**, 3019–23.

15 M. Gruber, V. Davesne, M. Bowen, S. Boukari, E. Beaurepaire, W. Wulfhekel and T. Miyamachi, *Phys. Rev. B*, 2014, **89**, 195415.

16 V. Davesne, M. Gruber, M. Studniarek, W. H. Doh, S. Zafeiratos, L. Joly, F. Sirotti, M. G. Silly, A. B. Gaspar, J. A. Real, G. Schmerber, M. Bowen, W. Weber, S. Boukari, V. Da Costa, J. Arabski, W. Wulfhekel and E. Beaurepaire, *J. Chem. Phys.*, 2015, **142**.

17 K. Bairagi, O. Iasco, A. Bellec, A. Kartsev, D. Li, J. Lagoute, C. Chacon, Y. Girard, S. Rousset, F. Miserque, Y. J. Dappe, A. Smogunov, C. Barreteau, M.-L. Boillot, T. Mallah and V. Repain, *Nat. Commun.*, 2016, **7**, 12212.

18 V. Shalabaeva, S. Rat, M. D. Manrique-Juarez, A.-C. Bas, L. Vendier, L. Salmon, G. Molnár and A. Bousseksou, *J. Mater. Chem. C*, 2017, **5**, 4419–4425.

19 T. Jasper-Tönnies, M. Gruber, S. Karan, H. Jacob, F. Tuczek and R. Berndt, *J. Phys. Chem. Lett.*, 2017, **8**, 1569–1573.

20 S. Ossinger, H. Naggert, L. Kipgen, T. Jasper-Toennies, A. Rai, J. Rudnik, F. Nickel, L. M. Arruda, M. Bernien, W. Kuch, R. Berndt and F. Tuczek, *J. Phys. Chem. C*, 2017, **121**, 1210–1219.

21 V. Shalabaeva, K. Ridier, S. Rat, M. D. Manrique-Juarez, L. Salmon, I. Séguy, A. Rotaru, G. Molnár and A. Bousseksou, *Appl. Phys. Lett.*, 2018, **112**, 13301.

22 K. Bairagi, A. Bellec, C. Fourmental, O. Iasco, J. Lagoute, C. Chacon, Y. Girard, S. Rousset, F. Choueikani, E. Otero, P. Ohresser, P. Sainctavit, M.-L. Boillot, T. Mallah and V. Repain, *J. Phys. Chem. C*, 2018, **122**, 727–731.

23 E. Ruiz, *Phys. Chem. Chem. Phys.*, 2014, **16**, 14–22.

24 J. S. Moodera, B. Koopmans and P. M. Oppeneer, *MRS Bull.*, 2014, **39**, 578–581.

25 C. Lefter, V. Davesne, L. Salmon, G. Molnár, P. Demont, A. Rotaru and A. Bousseksou, *Magnetochemistry*, 2016, **2**, 18.

26 J. Wang, Q. Liu, Y.-S. Meng, X. Liu, H. Zheng, Q. Shi, C. Duan and T. Liu, *Chem. Sci.*, 2018, **0**, 1–6.

27 K. Senthil Kumar and M. Ruben, *Coord. Chem. Rev.*, 2017, **346**, 176–205.

28 M. M. Khusniyarov, *Chem. - A Eur. J.*, 2016, **22**, 15178–15191.

29 A. Witt, F. W. Heinemann, S. Sproules and M. M. Khusniyarov,

Chem. - A Eur. J., 2014, **2**, 11149–11162.
30 A. Witt, F. W. Heinemann and M. M. Khusniyarov, *Chem. Sci.*, 2015, **6**, 4599–4609.
31 S. Venkataramani, *Science*, 2011, **445**, 445–448.
32 M. Dommaschk, M. Peters, F. Gutzeit, C. Schütt, C. Näther, F. D. Sönnichsen, S. Tiwari, C. Riedel, S. Boretius and R. Herges, *J. Am. Chem. Soc.*, 2015, **137**, 7552–7555.
33 G. Heitmann, C. Schütt, J. Gröbner, L. Huber and R. Herges, *Dalt. Trans.*, 2016, **45**, 11407–11412.
34 M.-L. Boillot, J. Zarembowitch and A. Sour, in *Spin Crossover in Transition Metal Compounds II*, ed. P. G. and H. A. Goodwin, Springer-Verlag Berlin Heidelberg, New York, 2004, pp. 261–276.
35 M.-L. Boillot, C. Roux, J.-P. Audière, A. Dausse and J. Zarembowitch, *Inorg. Chem.*, 1996, **35**, 3975–3980.
36 M. Nihei, Y. Suzuki, N. Kimura, Y. Kera and H. Oshio, *Chem. - A Eur. J.*, 2013, **19**, 6946–6949.
37 A. Bannwarth, S. O. Schmidt, G. Peters, F. D. Sönnichsen, W. Thimm, R. Herges and F. Tuczek, *Eur. J. Inorg. Chem.*, 2012, 2776–2783.
38 K. Sénéchal-David, N. Zaman, M. Walko, E. Halza, E. Rivière, R. Guillot, B. L. Feringa and M.-L. Boillot, *Dalton Trans.*, 2008, 1932–1936.
39 A. Tissot, M.-L. Boillot, S. Pillet, E. Codjovi, K. Boukheddaden and L. M. Lawson Daku, *J. Phys. Chem. C*, 2010, **114**, 21715–21722.
40 Y. Garcia, V. Ksenofontov, R. Lapouyade, A. D. Naik, F. Robert and P. Gütlich, *Opt. Mater. (Amst).*, 2011, **33**, 942–948.
41 J. Zarembowitch, C. Roux, M.-L. Boillot, R. Claude, J.-P. Itie, A. Polian and M. Bolte, *Mol. Cryst. Liq. Cryst. Sci. Technol. Sect. A. Mol. Cryst. Liq. Cryst.*, 1993, **234**, 247–254.
42 M. Milek, F. F. W. Heinemann and M. M. M. Khusniyarov, *Inorg. Chem.*, 2013, **52**, 11585–92.
43 B. Rösner, M. Milek, A. Witt, B. Gobaut, P. Torelli, R. H. Fink and M. M. Khusniyarov, *Angew. Chemie Int. Ed.*, 2015, **54**, 12976–12980.
44 K. Takahashi, Y. Hasegawa, R. Sakamoto, M. Nishikawa, S. Kume, E. Nishibori and H. Nishihara, *Inorg. Chem.*, 2012, **51**, 5188–5198.
45 Y. Hasegawa, S. Kume and H. Nishihara, *Dalton Trans.*, 2009, **2**, 280–284.
46 M. Irie, T. Fukaminato, K. Matsuda and S. Kobatake, *Chem. Rev.*, 2014, **114**, 12174–12277.
47 H. Naggert, J. Rudnik, L. Kipgen, M. Bernien, F. Nickel, L. M. Arruda, W. Kuch, C. Näther and F. Tuczek, *J. Mater. Chem. C*, 2015, **3**, 7870–7877.
48 G. Poneti, L. Poggini, M. Mannini, B. Cortigiani, L. Sorace, E. Otero, P. Sainctavit, A. Magnani, R. Sessoli and A. Dei, *Chem. Sci.*, 2015, **6**, 2268–2274.
49 G. Poneti, M. Mannini, B. Cortigiani, L. Poggini, L. Sorace, E. Otero, P. Sainctavit, R. Sessoli and A. Dei, *Inorg. Chem.*, 2013, **52**, 11798–805.
50 G. Félix, W. Nicolazzi, M. Mikolasek, G. Molnár and A. Bousseksou, *Phys. Chem. Chem. Phys.*, 2014, **16**, 7358.
51 M. Nishino, K. Boukheddaden, Y. Konishi and S. Miyashita, *Phys. Rev. Lett.*, 2007, **98**, 1–4.
52 A. Hauser, *Top. Curr. Chem.*, 2004, **234**, 155–198.
53 B. Warner, J. C. Oberg, T. G. Gill, F. El Hallak, C. F. Hirjibehedin, M. Serri, S. Heutz, M.-A. Arrio, P. Sainctavit, M. Mannini, G. Poneti, R. Sessoli and P. Rosa, *J. Phys. Chem. Lett.*, 2013, **4**, 1546–1552.
54 K. Burger, C. Furlani and G. Mattogno, *J. Electron Spectros. Relat. Phenomena*, 1980, **21**, 249–256.
55 M. S. Lazarus, M. A. Hoselton and T. S. Chou, *Inorg. Chem.*, 1977, **16**, 2549–2553.
56 E. C. Ellingsworth, B. Turner and G. Szulczewski, *RSC Adv.*, 2013, **3**, 3745.
57 Y. G. Borod'ko, S. I. Vetchinkin, S. L. Zimont, I. N. Ivleva and Y. M. Shul'ga, *Chem. Phys. Lett.*, 1976, **42**, 264–267.
58 L. Y. Johansson, R. Larsson, J. Blomquist, C. Cederström, S. Grapengiesser, U. Helgeson, L. C. Moberg and M. Sundbom, *Chem. Phys. Lett.*, 1974, **24**, 508–513.
59 J. Chastain and J. Moulder, *Handbook of x-ray photoelectron spectroscopy: a reference book of standard spectra for identification and interpretation of XPS data*, 1995.
60 N. Katsonis, T. Kudernac, M. Walko, S. J. van der Molen, B. J. van Wees and B. L. Feringa, *Adv. Mater.*, 2006, **18**, 1397–1400.
61 X. Zhang, T. Palamarciuc, P. Rosa, J. F. Létard, B. Doudin, Z. Zhang, J. Wang and P. A. Dowben, *J. Phys. Chem. C*, 2012, **116**, 23291–23296.
62 S. Tanaka, M. Toba, T. Nakashima, T. Kawai and K. Yoshino, *Jpn. J. Appl. Phys.*, 2008, **47**, 1215–1218.
63 J. Frisch, M. Herder, P. Herrmann, G. Heimel, S. Hecht and N. Koch, *Appl. Phys. A*, 2013, **113**, 1–4.
64 G. A. Bain and J. F. Berry, *J. Chem. Educ.*, 2008, **85**, 532.
65 J. J. Yeh and I. Lindau, *At. Data Nucl. Data Tables*, 1985, **32**, 1–155.
66 C. J. Mundy, F. Mohamed, F. Schiffman, G. Tabacchi, H. Forbert, W. Kuo, J. Hutter, M. Krack, M. Iannuzzi, M. McGrath, M. Guidon, T. D. Kuehne, J. Vandevondele, V. Weber and T. Laino, .
67 A. D. Becke, *Phys. Rev. A*, 1988, **38**, 3098–3100.
68 C. Lee, W. Yang and R. G. Parr, *Phys. Rev. B*, 1988, **37**, 785–789.
69 R. Sabatini, T. Gorni and S. de Gironcoli, *Phys. Rev. B*, 2013, **87**, 41108.
70 J. VandeVondele and J. Hutter, *J. Chem. Phys.*, 2007, **127**, 114105.
71 Y. Zhang and W. Yang, *Phys. Rev. Lett.*, 1998, **80**, 890–890.
72 M. Reiher, *Inorg. Chem.*, 2002, **41**, 6928–6935.